Published in final edited form as:
Chem Sci. 2013 ; 42: 220–225. doi:10.1039/C2SC21074F.

Enzymatic activation of nitro-aryl fluorogens in live bacterial cells for enzymatic turnover-activated localization microscopy†

Marissa K. Lee[a], **Jarrod Williams**[b], **Robert J. Twieg**[b], **Jianghong Rao**[c], and **W. E. Moerner**[a]
[a]Department of Chemistry, Stanford University, Stanford, California 94305, USA. wmoerner@stanford.edu

[b]Department of Chemistry and Biochemistry, Kent State University, Kent, Ohio, 44240, USA

[c]Department of Radiology, Stanford University, Stanford, California 94305, USA

Abstract

Many modern super-resolution imaging methods based on single-molecule fluorescence require the conversion of a dark fluorogen into a bright emitter to control emitter concentration. We have synthesized and characterized a nitro-aryl fluorogen which can be converted by a nitroreductase enzyme into a bright push–pull red-emitting fluorophore. Synthesis of model compounds and optical spectroscopy identify a hydroxyl-amino derivative as the product fluorophore, which is bright and detectable on the single-molecule level for fluorogens attached to a surface. Solution kinetic analysis shows Michaelis–Menten rate dependence upon both NADH and the fluorogen concentrations as expected. The generation of low concentrations of single-molecule emitters by enzymatic turnovers is used to extract subdiffraction information about localizations of both fluorophores and nitroreductase enzymes in cells. Enzymatic Turnover Activated Localization Microscopy (ETALM) is a complementary mechanism to photoactivation and blinking for controlling the emission of single molecules to image beyond the diffraction limit.

Introduction

Recently developed microscopies (*e.g.*, PALM, FPALM, STORM) bypass the optical diffraction limit (DL) by successive imaging and localization of sparse subsets of single-molecule (SM) fluorophores.[1–3] Using these “superresolution” (SR) imaging methods, structures can be imaged with spatial resolution 5–10 times smaller than the DL of ≈200 nm for visible wavelengths. Bright emitters are essential for this SR strategy, because the localization resolution improves as $1/\sqrt{N}$, with N the number of photons detected before photobleaching or per switching cycle.[4] Using emitters whose concentration can be controlled ensures that each frame during an acquisition has only a sparse set of emitting molecules, even if the object of interest is densely labelled.[5] Though most previous SR experiments in cells have used photocontrollable fluorescent proteins (FPs)[6–8] because of their genetic targeting capabilities, these emit (on average) 10-fold fewer photons before photobleaching than good small-molecule fluorophores.[5] Targeting small organic fluorophores to specific cellular locations[9,10] has been developed as an alternative to FPs,

Correspondence to: W. E. Moerner.

† Electronic supplementary information (ESI) available: Full experimental details, product characterization, selected NMR spectra, and additional figures are provided.

‡ Since many nitro compounds are known to be toxic to bacterial cells,[20] the total time of SR experiments from addition of **1** to imaging was kept as short as possible (<10 minutes).

and although challenges remain for cell entry and washout, the chemical properties, spectral range, and photophysics are more readily modified by organic synthesis.[11]

For SR imaging, the emission from organic fluorophores can be controlled optically by reversible photoswitching[12] (often in the presence of additives like thiols, or oxidizing/reducing agents)[3,13,14] or by irreversible photoactivation.[15] Non-optical methods to control fluorescence emission include ligand binding,[16] and fluorescence quenchers.[17] Fluorogenic substrates have enabled detailed single-molecule enzymology studies[18] but without extracting subdiffraction information. We present a small-molecule fluorophore synthetically modified to form an enzymatically activated and cell-permeable fluorogen, and demonstrate Enzymatic Turnover Activated Localization Microscopy (ETALM), a new SR imaging method, in bacterial cells. ETALM differs from other fluorescence modulation strategies using a chemical reduction[19] because the enzymatic turnover continually generates new fluorophores. This activation is irreversible and the new fluorophores do not undergo multiple switching cycles. The emitting concentration can be set at the required low level for SR imaging simply by limiting the fluorogen concentration or slowing the enzymatic rate using inhibitors.

Nitroreductase (NTR) enzymes are a family of NAD(P)H-dependent flavoproteins ubiquitous in bacteria and capable of reducing aryl-nitro compounds to their corresponding hydroxyl-amino or amino derivatives.[20,21] Previous work has used a NTR enzyme to reduce a nitro-fluorogen into a cancer therapeutic[22–24] but the resulting fluorophore was not sufficiently bright or emitted at too short a wavelength to allow SM imaging in cells. This study uses the commercially available *E. coli nsfB* NTR[21] (>90 % pure, see ESI Fig. S1†) which has been well-studied because of its potential use in cancer therapeutic delivery.[25]

We show below that NTR converts the nitro-aryl fluorogen of the present study **1** into a bright organic fluorophore, suitable for SR in live bacterial cells (Scheme 1). The emissive product belongs to the dicyanomethylenedihydrofuran (DCDHF) class of push–pull fluorophores where an electron-poor DCDHF acceptor head is connected to an electron-rich donor, usually an amine, through a conjugated π network.[26] The DCDHF fluorophores are detectable on the SM level because they emit millions of photons before photobleaching and have high fluorescence quantum yields in viscous environments, including membranes and gelatin.[27] Importantly, DCDHF fluorophores can enter living cells fairly easily because they are neutral, and they emit at long wavelengths to avoid autofluorescence.[27]

Results and discussion

We previously reported a photoactivatable azido-DCDHF[15,28] suitable for SR in bacterial and mammalian cells.[29] To create another dark DCDHF fluorogen, the electron-rich amine of the emissive form can be replaced with an electron-poor nitro group which eliminates fluorescence and shifts the absorbance to the blue. Then, reduction of **1** in buffer by the NTR enzyme in the presence of NADH creates the red-shifted emitter (Fig. 1).

The product fluorophore in these bulk spectroscopic measurements could be either the hydroxyl-amino-DCDHF **2** or the amino-DCDHF **3** (Scheme 1). The product of the NTR reaction was determined to be **2** instead of **3** by comparing the bulk emission and excitation spectra (in buffer) of separately synthesized **2** and **3** with the reaction mixture (Fig. 1B). There is close spectral overlap between the NTR reaction mixture product and **2**.

The bulk and SM photophysical characteristics of molecules **1–3** were measured in solution and in a polymer film (Table 1). Solution measurements were performed in ethanol on purified compounds to allow comparison with our previously published work on DCDHF-type fluorophores.[15] A poly-(methylmethacrylate) (PMMA) polymer film in toluene was

used in a bulk spectroscopic measurement to show the increase of fluorescence quantum yield (Φ_F) of **2** and **3** in more rigid environments. PMMA polymers, though used previously to characterize the azido-DCDHF fluorogen,[15] are less relevant to behaviour inside a cell, but measurements were performed in PMMA to compare **2** to prior work. As is the case for the other DCDHF fluorophores,[26] the fluorescence quantum yield Φ_F of **2** increases in the more constrained polymer environment. In order to assess the potential of **2** for cell imaging, more biologically relevant conditions were used for microscopy measurements of the photobleaching quantum yield (Φ_B) and the average number of total photons emitted (N_{tot}). Here, we used a primarily aqueous polymer film (1% poly(vinyl alcohol) (PVA) in water) to immobilize the fluorophores. Other *in vitro* environments like poly-lysine or gelatin either did not provide sufficient immobilization, or had an unacceptably high fluorescence background at the wavelengths used.

Importantly for single-molecule based superresolution imaging strategies, SMs of **2** were detectable when immobilized in the aqueous PVA polymer film (Fig. 2A), confirmed by the observation of single-step photobleaching to the background level. Movie S1† shows SMs of **2** in PVA, and representative time traces of the SMs appear in Fig. S7.† The average number of photons detected before photobleaching (N_{tot}) was measured for **2** and **3** (Fig. 2A and B, Table 1) using the survival probability. The survival probability P_N (Fig. 2B) is the ratio of the number of SMs m_n surviving after a given number of emission events N to the total number of molecules M in the measurement set (see ESI†).[15,30] This approach gives comparable results to histogramming the detected photons[31] but avoids binning artifacts. To convert photons detected to total emitted photons, the detected value is divided by the optical system collection efficiency[32] of 0.04.

After photophysical characterization of separately synthesized **1–3**, we used microscopy to measure the fluorescence generated by the NTR-reaction on a surface *in vitro*. Compound **4**, a *N*-hydroxy-succinimide (NHS) derivative of **1** (Chart 1) was covalently attached to poly-lysine coated coverslips through reaction of NHS with the surface amines. After washing off the unreacted **4**, NADH and NTR enzyme were added in buffer and allowed to react with the attached **4**. Dramatic fluorescence turn-on was observed after this addition (Fig. 2D and inset).

Our microscopy-based experiments could detect SMs of **2** and see fluorescence from the NTR-reaction, but do not quantify the NTR reaction rate. We used bulk spectroscopic measurements in solution to find the NTR reaction kinetic rates (Fig. 3) and used the more water-soluble nitro derivative **5** (Chart 1) instead of **1** because **1** aggregates in higher concentration regimes. (Kinetic measurements using **1** at lower concentrations are shown in the ESI, Fig S8†). NTR follows a ping-pong bi–bi mechanism[33] (eqn (1)) where the rate per enzyme (ν_i/E) depends on both NADH and nitro substrate **5** concentrations with two Michaelis constants:[34,35]

$$\frac{\nu_i}{E} = \frac{k_{cat}[5][\mathrm{NADH}]}{K_m^{[5]}[\mathrm{NADH}] + K_m^{\mathrm{NADH}}[5] + [5][\mathrm{NADH}]} \quad (1)$$

The initial rate of product formation, monitored by absorption at 500 nm, was measured for a range of initial concentrations of **5** and NADH (Fig. 3). These rates were fit to eqn (1), yielding fit parameters k_{cat} of 224 ± 40 s^{-1} and K_M^{NADH} of 13 ± 3 μM and a $K_M^{[5]}$ of 4.9 ± 1 μM, consistent with prior work.[34]

After confirming the NTR-reaction fluorescence turn-on on a surface and measuring the bulk NTR rate, we explored the NTR-reaction scheme for turnover of the fluorogen in

bacterial cells. NTR enzymes are endogenous in many bacteria. When several bacterial species (*E. coli, Caulobacter crescentus, Bacillus subtilis*) are incubated with μM concentrations of **1**, entire cells become fluorescent (Fig. 4A and ESI Fig S9†). This effect was most dramatic in wild type *B. subtilis* cells, which are known to have enhanced response to nitro compounds.[36,37] To support the hypothesis that this fluorescence arises from a NTR reduction analogous to the reaction studied *in vitro*, **1** and an excess of menadione, a competitive NTR inhibitor, were added simultaneously to the bacteria. Under this incubation condition, the fluorescence of individual cells was reduced by 14× to just above background levels (Fig. 4B and E). No additives were needed to make **1** cell permeable.

When *B. subtilis* cells are incubated with 5 μM concentrations of **1**, the emission spots from the large number of enzymatically generated diffusing fluorophores overlap, and the cells appear bright so that distinct single molecules cannot be observed. By lowering the incubation concentration of **1** to <nM levels, separated fluorescent spots can be observed turning on and subsequently photobleaching (Fig. 5A and insets). Even though the true size of the emitting molecule is ≈1 nm, the diameter of the SM fluorescent spot is ≈200 nm, on the order of the bacterial cell width, due to the DL. These fluorescent spots correspond to SMs, verified by one step photobleaching to background levels. At the laser intensity used here (15 kW cm^{-2}), photobleaching is fast relative to the 100 ms exposure time, as shown by representative time-traces of the SM emission (Fig. 5A).

We now seek to demonstrate that SR information can be extracted from the enzyme turnovers using ETALM.‡ As is well-known, with separated SM fluorophores, the fitted center of the DL spot is an estimate of the true position of the emitting molecule. By lowering the incubation concentration, the total number of enzymatically generated fluorophores is easily decreased. The incubation concentration of **1** used to create Fig. 5A was slightly too low for SR imaging, as only one SM spot would appear in a given DL region every 8–30 seconds. The incubation concentration of **1** was increased very slightly to 1.5 nM, so new SMs were generated at a reasonable rate during continuous imaging. A DL image composed of the average of many imaging frames is shown in Fig. 5B. It should be noted that our interpretation of SR reconstructions could still be complicated by blurred spots arising from diffusion of the free fluorophores after catalysis. To minimize this effect, the number of long-lived fluorophores is reduced by using high intensity reading light, and the camera exposure time is reduced to 8 ms per frame. In the limit of very high laser intensity, each newly generated SM fluorophore should be photobleached before it has time to diffuse away from the NTR enzyme. In this limit, the extracted SM positions would be samplings of the NTR enzyme position over time as it moves through the cell, generating fluorescent molecules. In this initial demonstration, we only approached this limit in intensity, thus in our SR reconstructions (Fig. 5C–F and Movie S2†), two populations of localizations are observed: (i) punctate spots (dashed boxes in Fig. 5C and E) and (ii) membrane localizations (*e.g.*, seen easily in Fig. 5C). For case (i), aggregation could cause the punctate spots, but **1** is added at the nM level and was only found to aggregate at the μM regime in separate experiments. We hypothesize that the punctate spots arise from a “cloud” of enzymatically generated fluorophores photobleached before they could travel very far from the enzyme. Notably, time-coloring of the successive SM localizations from the fluorescence movie sometimes shows apparent motion of the enzyme (Fig. 5F). Considering the second population (ii), some emitters can apparently survive for a longer time and are able to diffuse to reach the membrane which represents a sink for the relatively nonpolar **2**. It is reasonable that a small fraction of fluorophores could reach the protective environment of the membrane without photobleaching given that the expected diffusion coefficient for a small molecule in a bacterial cell is on the order of 5.0×10^{-7} cm^2 s^{-1},[38] which could easily result in an rms displacement of 1.5 microns during the 8 ms imaging time. Membrane-

bound fluorophores are more easily localized because diffusion is slower[39] and the DCDHF-type fluorophores are harder to bleach (since ΦF is larger in the membrane).[27]

Conclusions

We have synthesized and characterized a nitro-fluorogen which can be enzymatically activated to produce a bright SM emitter. The fluorescent product was identified and characterized on a bulk and SM-level *in vitro* and in cells. Unlike previous work using enzymatic turnovers to generate fluorescent SM products,[40–42] we used the nascent fluorescent molecules from the NTR enzyme on the single-molecule level to explore the subdiffraction-scale organization of a cytosolic bacterial enzyme in *B. subtilis* as well as the membrane locations where some of the product molecules are found.

Considering extensions beyond bacteria, mammalian cells often have much lower levels of NTR-type enzymes[20] or activity and would be interesting targets for future work. In cells with suitably low levels of endogenous NTR activity, the ETALM scheme could be used as an orthogonal genetically encoded strategy for SR imaging of protein structures of interest fused to NTR. One particular advantage of this approach arises from the fact that the precursor nitro-fluorogen **1** is not fluorescent, so no washing steps are required. The activation of **1** is not light-dependent, and samples do not require special handling under red lights or in the dark. It may be useful in some contexts to use the NTR scheme as a generator of fluorescent molecules from a source inside the bacterial cell to obtain the position of the inner membrane.[43] At the same time, one of the challenges of this system is controlling the total amount of activated fluorophores. We used high intensity laser light to rapidly bleach nascent fluorophores, but the use of an inhibitor could also allow temporary suppression and tuning of the fluorescence generation rate.

Supplementary Material

Refer to Web version on PubMed Central for supplementary material.

Acknowledgments

This work was supported in part by grant no. R01-GM086196 from the National Institute of General Medical Sciences. Samples of wild-type *Bacillus subtilis, E. coli,* and *Caulobacter crescentus* were obtained from Jerod Ptacin in the Shapiro lab at Stanford University. The protein gel was run with the help of Steffi Duttler in the Frydman lab at Stanford University.

Notes and references

1. Betzig E, Patterson GH, Sougrat R, Lindwasser OW, Olenych S, Bonifacino JS, Davidson MW, Lippincott-Schwartz J, Hess HF. Science. 2006; 313:1642–1645. [PubMed: 16902090]
2. Hess ST, Girirajan TPK, Mason MD. Biophys. J. 2006; 91:4258–4272. [PubMed: 16980368]
3. Rust MJ, Bates M, Zhuang X. Nat. Methods. 2006; 3:793–796. [PubMed: 16896339]
4. Thompson RE, Larson DR, Webb WW. Biophys. J. 2002; 82:2775–2783. [PubMed: 11964263]
5. Lord SJ, Lee HD, Moerner WE. Anal. Chem. 2010; 82:2192–2203. [PubMed: 20163145]
6. Dickson RM, Norris DJ, Tzeng YL, Moerner WE. Science. 1996; 274:966–969. [PubMed: 8875935]
7. Patterson GH, Lippincott-Schwartz J. Science. 2002; 297:1873–1877. [PubMed: 12228718]
8. Ando R, Mizuno H, Miyawaki A. Science. 2004; 306:1370–1373. [PubMed: 15550670]
9. Fernandez-Suarez M, Ting AY. Nat. Rev. Mol. Cell Biol. 2008; 9:929–943. [PubMed: 19002208]
10. George N, Pick H, Vogel H, Johnsson N, Johnsson K. J. Am. Chem. Soc. 2004; 126:8896–8897. [PubMed: 15264811]

11. Maurel D, Banala S, Laroche T, Johnsson K. ACS Chem. Biol. 2010; 5:507–516. [PubMed: 20218675]
12. Fölling J, Belov V, Kunetsky R, Medda R, Schönle A, Egner A, Bossi M, Hell SW. Angew. Chem., Int. Ed. 2007; 46:6266–6270.
13. Dempsey GT, Vaughan JC, Chen KH, Bates M, Zhuang X. Nat. Methods. 2011; 8:1027–1036. [PubMed: 22056676]
14. Heilemann M, van de Linde S, Schüttpelz M, Kasper R, Seefeldt B, Mukherjee A, Tinnefeld P, Sauer M. Angew. Chem., Int. Ed. 2008; 47:6172–6176. DOI: 10.1002/anie.200802376.
15. Lord SJ, Conley NR, Lee HD, Samuel R, Liu N, Twieg RJ, Moerner WE. J. Am. Chem. Soc. 2008; 130:9204–9205. DOI: 10.1021/ja802883k. [PubMed: 18572940]
16. Sharonov A, Hochstrasser RM. Proc. Natl. Acad. Sci. U. S. A. 2006; 103:18911–18916. [PubMed: 17142314]
17. Schwering M, Kiel A, Kurz A, Lymperopoulos K, Sprödefeld A, Kramer R, Herten D. Angew. Chem., Int. Ed. 2011; 50:2940–2945.
18. English BP, Min W, van Oijen AM, Lee KT, Luo G, Sun H, Cherayil BJ, Kou SC, Xie XS. Nat. Chem. Biol. 2006; 2:87–94. [PubMed: 16415859]
19. Vogelsang J, Cordes T, Forthmann C, Steinhauer C, Tinnefeld P. Proc. Natl. Acad. Sci. U. S. A. 2009; 106:8107–8112. DOI: 10.1073/pnas.0811875106. [PubMed: 19433792]
20. Roldán MD, Pérez-Reinado E, Castillo F, Vivián CM. FEMS Microbiol. Rev. 2008; 32:474–500. [PubMed: 18355273]
21. Anlezark G, Melton R, Sherwood R, Coles B, Friedlos F, Knox R. Biochem. Pharmacol. 1992; 44:2289–2295. [PubMed: 1472094]
22. Hodgkiss RJ, Begg AC, Middleton RW, Parrick J, Stratford ML, Wardman P, Wilson GD. Biochem. Pharmacol. 1991; 41:533–541. [PubMed: 1705123]
23. Liu Y, Xu Y, Qian X, Xiao Y, Liu J, Shen L, Li J, Zhang Y. Bioorg. Med. Chem. Lett. 2006; 16:1562–1566. [PubMed: 16403630]
24. Thorne SH, Barak Y, Liang W, Bachmann MH, Rao J, Contag CH, Matin A. Mol. Cancer Ther. 2009; 8:333–341. [PubMed: 19190118]
25. Green NK, Kerr DJ, Mautner V, Harris PA, Searle PF. Methods Mol. Med. 2004; 90:459–477. [PubMed: 14657579]
26. Willets KA, Nishimura SY, Schuck PJ, Twieg RJ, Moerner WE. Acc. Chem. Res. 2005; 38:549–556. [PubMed: 16028889]
27. Lord SJ, Conley NR, Lee HD, Nishimura SY, Pomerantz AK, Willets KA, Lu Z, Wang H, Liu N, Samuel R, Weber R, Semyonov AN, He M, Twieg RJ, Moerner WE. ChemPhysChem. 2009; 10:55–65. DOI: 10.1002/cphc.200800581. [PubMed: 19025732]
28. Lord SJ, Lee HD, Samuel R, Weber R, Liu N, Conley NR, Thompson MA, Twieg RJ, Moerner WE. J. Phys. Chem. B. 2010; 114:14157–14167. [PubMed: 19860443]
29. Lee HD, Lord SJ, Iwanaga S, Zhan K, Xie H, Williams JC, Wang H, Bowman GR, Goley ED, Shapiro L, Twieg RJ, Rao J, Moerner WE. J. Am. Chem. Soc. 2010; 132:15099–15101. DOI: 10.1021/ja1044192. [PubMed: 20936809]
30. Molski A. J. Chem. Phys. 2001; 114:1142–1147. DOI: 10.1063/1.1333760.
31. Lounis BL, Orrit M. Rep. Prog. Phys. 2005; 68:1129–1179.
32. Moerner WE, Fromm DP. Rev. Sci. Instrum. 2003; 74:3597–3619.
33. Cleland W. Biochim. Biophys. Acta. 1963; 67:104–137. [PubMed: 14021667]
34. Jarrom D, Jaberipour M, Guise C, Daff S, White S, Searle P, Hyde E. Biochemistry. 2009; 48:7665–7672. [PubMed: 19580253]
35. Race P, Lovering A, Green R, Ossor A, White S, Searle P, Wrighton C, Hyde E. J. Biol. Chem. 2005; 280:13256–13264. [PubMed: 15684426]
36. Mostertz J, Scharf C, Hecker M, Homuth G. Microbiology. 2003; 150:497–512. [PubMed: 14766928]
37. Van Duy N, Wolf C, Mäader U, Lalk M, Langer P, Lindequist U, Hecker M, Antelmann H. Proteomics. 2007; 7:1391–1408. [PubMed: 17407181]

38. Mika JT, van den Bogaart G, Veenhoff L, Krasnikov V, Poolman B. Mol. Microbiol. 2010; 77:200–207. [PubMed: 20487282]

39. Nishimura SY, Lord SJ, Klein LO, Willets KA, He M, Lu Z, Twieg RJ, Moerner WE. J. Phys. Chem. B. 2006; 110:8151–8157. DOI: 10.1021/jp0574145. [PubMed: 16610918]

40. Smiley RD, Hammes GG. Chem. Rev. 2006; 106:3080–3094. DOI: 10.1021/cr0502955 er. [PubMed: 16895319]

41. Roeffaers M, Cremer GD, Libeert J, Ameloot R, Dedecker P, Bons A, Bückins M, Martens J, Sels B, De Vos D, Hofkens J. Angew. Chem., Int. Ed. 2009; 121:9449–9453.

42. Yoon H, Shim S, Baek L, Hong J. Bioorg. Med. Chem. Lett. 2011; 21:2403–2405. [PubMed: 21396812]

43. Lew MD, Lee SF, Ptacin JL, Lee MK, Twieg RJ, Shapiro L, Moerner WE. Proc. Natl. Acad. Sci. U. S. A. 2011; 108:E1102–E1110. DOI: 10.1073/pnas.1114444108. [PubMed: 22031697]

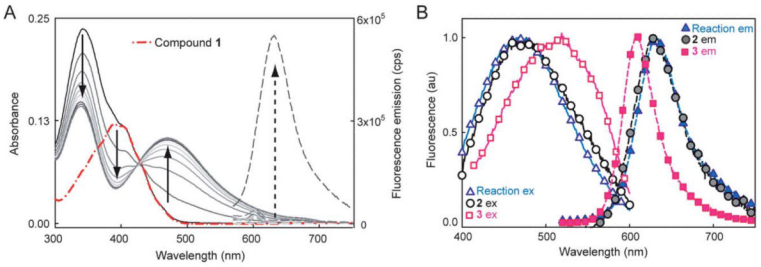

Fig. 1.

(A) Spectral change during the NTR reaction with **1** and NADH over ≈10 minutes showing red-shifted absorption and fluorescence increase. Solid curves show absorbance of the reaction mixture at different time points, broken red curve is absorbance of **1** alone. Dashed lines are fluorescence emission (500 nm excitation) before and after the NTR reaction. No fluorescence turn-on or absorbance change is observed without all three components, see ESI Fig. S2 and S3.† (B) Normalized excitation (solid curves and empty symbols, collected at emission max) and emission (dashed curves and solid symbols, 500 nm excitation) spectra of NTR reaction mixture (triangles) compared to separately synthesized **2** (circles) and **3** (squares). All spectra measured in 10 mM Tris–HCl (pH 7.5), for more details, see ESI.†

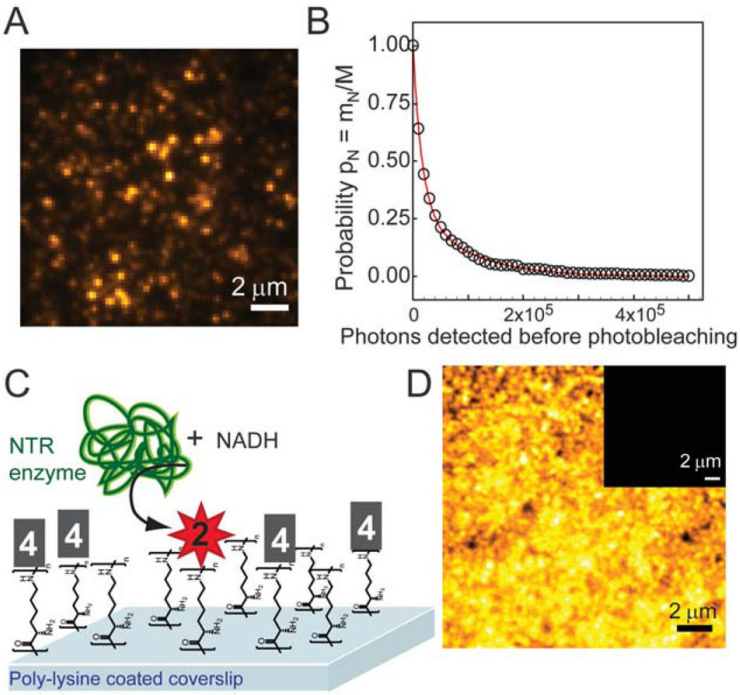

Fig. 2.

(A) SM fluorescent spots of **2** (verified by one-step photo-bleaching) in PVA film (532 nm excitation, 91 W cm^{-2}). (B) Survival probability histogram of **2** doped into PVA films at nM concentrations with an average 71 000 detected photons, corresponding to an average of 1.7 × 10^6 photons emitted by each SM. (C) Schematic of *in vitro* experiment where **4** (structure shown in Chart 1) was covalently attached to poly-lysine coverslips immersed in PBS buffer (pH 7.4) containing free NADH and NTR enzyme. Enzymatically generated fluorophores remained attached to surface lysines. (D) Bulk fluorescence at the surface after NADH and NTR addition. Inset: bulk fluorescence of **4** before NTR reaction (same contrast). Bulk fluorescence of all control incubation conditions is shown in Fig. S6.† sample and control details in ESI.†

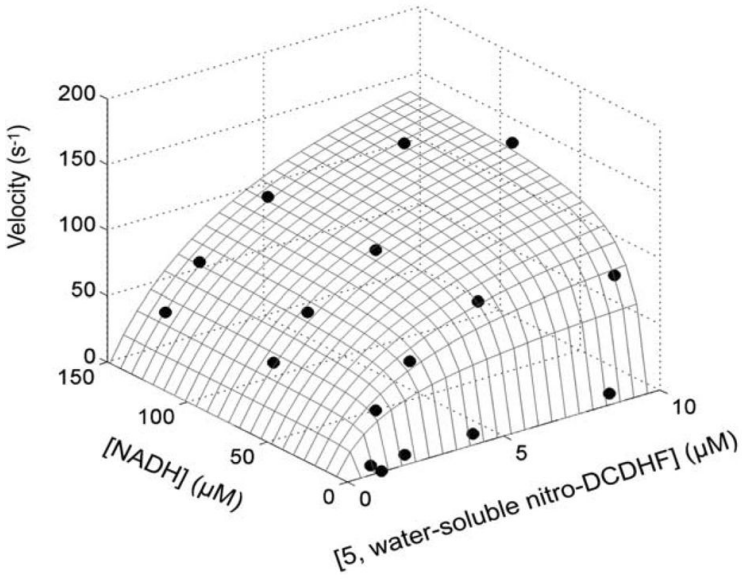

Fig. 3.

3D Michaelis–Menten plot of initial rate of product formation (monitored by change in absorption at 500 nm) in PBS (pH 7.4) *versus* various starting concentrations of **5** and NADH. The structure of **5** is shown in Chart 1. The grid is the fit of eqn (1) to the data points.

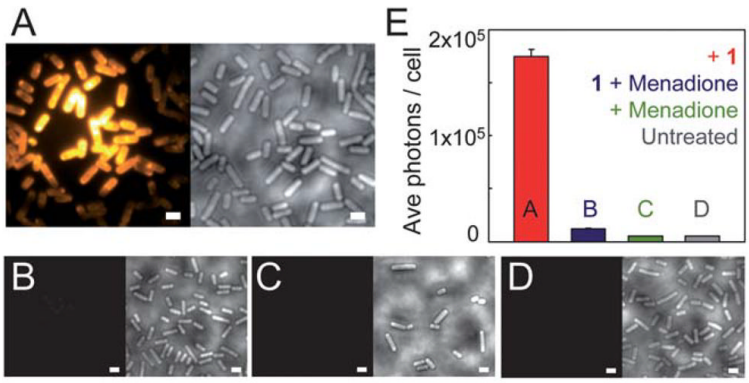

Fig. 4.

(A) *B. subtilis* incubated with 5 μM of **1**. Left image: average fluorescence; right image: corresponding white light image of cells. All cells become fluorescent; cells in the center are brighter because the laser excitation spot is more intense in the center. Images in the controls (B)–(D) are structured similarly: left image is average fluorescence at same contrast scale as (A), and right image is corresponding white light image. (B) *B. subtilis* incubated with both **1** (5 μM) and menadione (0.2 mM), showing a dramatic fluorescence reduction. The images in (C) show cells incubated with only menadione, and part (D) shows untreated *B. subtilis*. (E) Quantification of number of photons detected per cell (~300 cells per condition) for each case. All scale bars are 2 μm, imaging intensity is 2.5 kW cm^{-2}. All conditions were incubated for 30 minutes. For more details on incubation and imaging conditions, see ESI.†

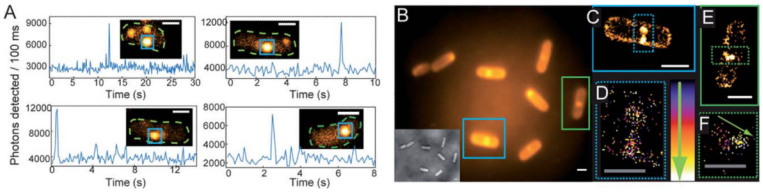

Fig. 5.

(A) Representative SM emission traces of enzymatically generated fluorophores in *B. subtilis* showing photons detected per 100 ms bin *vs.* time. For each graph, the inset is a single imaging frame from the specific *B. subtilis* cell (cell outline in dashed green, SM plotted is in blue box). (B) DL average image of 3000 frames (24 s) of *B. subtilis* incubated with **1** and corresponding white light image (inset). (C) SR reconstruction (average 17.9 ± 0.3 nm statistical precision) from the cell boxed in blue with both membrane localizations and punctate spots (blue dashed) consisting of many overlapping localizations. (D) Temporal progression of the localizations in the punctate spots, with early localizations colored purple, and later localizations colored white. The lack of temporal progression in the localizations suggests that these punctate spots correspond to the fluorescent cloud generated by two relatively stationary enzymes. (E) SR reconstruction from the green-boxed cell. (F) Temporal progression of localizations in the green dashed box of (E) showing a defined temporal progression with later localizations toward the center of the cell (shown by arrow), suggesting that this punctate spot is a single enzyme diffusing on the time scale of our experiment. Scale bars: 1 μm except 0.5 μm in (D and F). For more details on incubation, imaging, fitting, and display conditions, see the ESI.†

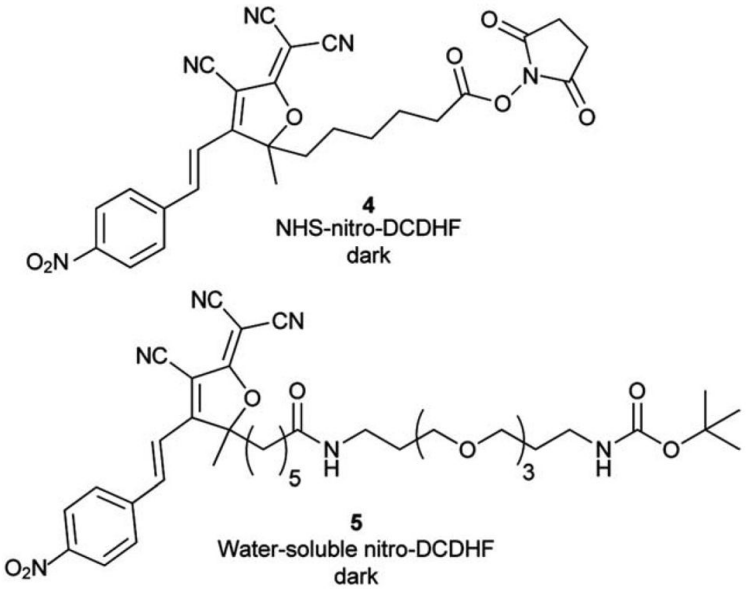

Chart 1.

Structures of nitro-DCDHF derivatives **4** and **5** used for surface immobilization and kinetic experiments, respectively. Bulk absorbance and fluorescence changes from the NTR reaction are shown in ESI Fig. S4 and Fig. S5, respectively.† Table S1 in ESI† summarizes photophysical characteristics for these molecules.

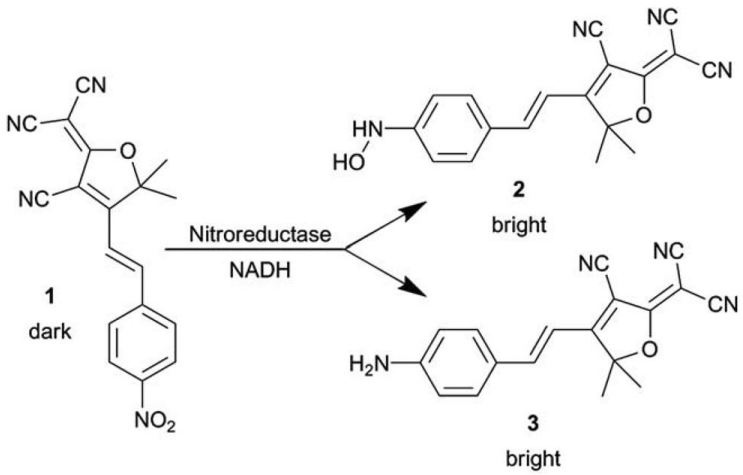

Scheme 1.
Reaction of **1** with NTR and NADH.

Table 1

Photophysical characterization of molecules 1–3 in ethanol (unless otherwise stated)[a]

	λ_{abs} (nm), ε ($dm^3\ mol^{-1}\ cm^{-1}$)	λ_{fl} (nm)	Φ_F	Φ_B[b] ($\times 10^{-6}$)	SM N_{tot}[c] ($\times 10^6$)
1	390, 17 020	n/a	n/a	n/a	n/a
2	497, 15 300	609	0.021, 0.27[d]	5.6	1.7
3	570, 54 100	613	0.025, 0.39[d]	4.1	2.3

[a] See ESI† and ref. 28 for details on measurements and calculations.

[b] Bulk quantum yield of permanent photobleaching, measured in aqueous PVA polymer film.

[c] Average total number of photons emitted for SMs in PVA polymer film.

[d] Fluorescence quantum yield in PMMA.